Field Emitted Electron Trajectories for the CEBAF Cavity*

Byung C. Yunn and Ronald M. Sundelin
Continuous Electron Beam Accelerator Facility
12000 Jefferson Avenue, Newport News, VA 23606, USA

Abstract

Electromagnetic fields of the superconducting 5-cell CEBAF cavity with its fundamental power coupler are solved numerically with URMEL and MAFIA codes. Trajectories of field emitted electrons following the Fowler-Nordheim relation are studied with a numerical program which accepts the URMEL/MAFIA fields. Emission sites and gradients are determined for those electrons which can reach the cold ceramic window either directly or by an energetic back-scattering. The peak and average impact energy and current are found. The generation of dark current by field emitted electrons has also been studied, and its relevance to CEBAF operation is briefly discussed.

I. INTRODUCTION

There are two principal reasons for interest in studying trajectories of field emitted electrons and of energetic back-scattered electrons. One would like to know what emission sites and gradients can result in electrons reaching the cold ceramic window. There have been several instances of breakdown of this window at CEBAF when rf powered. A speculation that field emitted electrons might be the cause of this damage has provided an initial motivation to this study. It is also interesting to find out under what conditions field emitted electrons could be accelerated the full length of the accelerator and constitute a halo to the beam. Some of the experiments planned at CEBAF require only a few nA beam currents. Depending on the circumstances, dark currents could become a detrimental noise source to such experiments, if not eliminated before reaching the experimental halls.

II. TRACKING ELECTRON TRAJECTORIES

As an analytical treatment of trajectories of field emitted electrons from the cavity surface is almost impossible, we decided to study them numerically. The trajectory of an electron under the influence of external electromagnetic fields is followed numerically providing information on the position and the momentum of the electron at any given instant. When an electron collides with the cavity surface made of niobium, a large fraction of incident energy may be carried away by a back-scattered electron. At the same time, secondary emission from the surface is responsible for low energy electrons with energies typically less than 50 eV. Those electrons are also followed until all particles generated are processed. The computer code we developed for this purpose is based on the MULPAC program[1], although most subroutines have to be rewritten to adapt to the change of input files now prepared with the electromagnetic field codes, URMEL and MAFIA instead of LALA. Particle pushing is also simplified adopting the Runge-Kutta method of order four. The Adams fourth-order predictor-corrector algorithm was used in the MULPAC code. We find it more expedient to improve on accuracy, if necessary, by reducing the size of a fixed time step rather than dynamically adjusting the step size constantly by correcting the prediction of the Adams-Bashforth four step method with the Adams-Moulton three step algorithm. MULPAC's back-scattering and secondary emission routines, however, remain unchanged. Presently, boundary checking routines for a portion of a structure, which require M3 generated mesh data, are to be tailor-made for each specific problem.

III. CALCULATION OF FIELDS

Electromagnetic fields excited in the CEBAF cavity powered from a klystron are calculated with the computer codes URMEL and MAFIA[2]. The properties of resonant modes of the 5-cell CEBAF cavity without the fundamental power coupler(FPC) were estimated with URMEL in detail[3], with a good agreement to measured data[4]. For the operating π mode, some URMEL results are: frequency is 1492.85 MHz, R/Q is 964.77 Ω/m, the ratio of peak surface electric field to the gradient is 2.24 found near the irises.

The FPC is located at the beam tube 3.17 cm away from an end-cell. It consists of two rectangular waveguides of different widths, 13.44 cm and 7.90 cm respectively, but of the same height of 2.54 cm. External Q of the cavity is adjusted by varying the location of the transition from narrow-width to wide-width waveguide. The input coupling goes through a minimum as the waveguide transition is moved. The FPC breaks the cylindrical symmetry of the structure requiring a 3-D code to investigate this cavity-waveguide coupled system. A further complication is that the resonant mode of interest is above the TE_{10} cutoff frequency, which is at 1115.19 MHz. The proper position of a waveguide short, necessary in any frequency domain code, is determined to be at a location 20.70 cm from the cavity centerline, which is a quarter-wavelength away from the detuned short. A consistency check on the numerically computed fields is based on the following observation. The ratio of the peak electric energy density in the FPC to the peak electric stored energy density in the center of the cavity cell is measured to be nearly independent of both the coupling strength and of the passband mode. For the π mode at a nominal Q_{ext} of 6.6×10^6, the reported value of this ratio is 0.0282. As it turns out to

*Supported by D.O.E. contract #DE-AC05-84ER40150.

0-7803-1203-1/93$03.00 © 1993 IEEE

be impractical to solve the whole 5-cell cavity-FPC structure, we divide the problem into two: a 5-cell cavity with the axial symmetry and one end-cell plus the FPC coupled system. An input to the trajectory program is then constructed with the MAFIA fields for the FPC including the section of beam pipe attached to the end cell, and the URMEL fields for the 5-cell cavity.

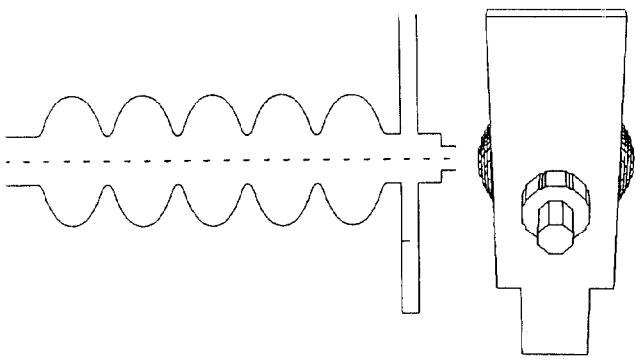

Figure 1. Cross-sectional view of 5-cell CEBAF cavity with the FPC and the front view of the FPC.

It is to be mentioned that higher order mode couplers also break the axial symmetry of the 5-cell cavity, further contaminating the fundamental mode with higher order modes. However, these effects are much weaker, and we neglect their presence for the study reported in this paper.

IV. RESULTS

The theory of field emission mechanism formulated by Fowler-Nordheim[5] describes the quantum mechanical tunneling of electrons through the modified potential barrier at the surface of a metal in a high external electric field. The field electron emission current density J in A/m^2 is given by

$$J = \frac{1.54 \times 10^6 (\beta E_{\rm surf})^2}{\phi} \exp\left(-\frac{6.83 \times 10^3 \phi^{1.5}}{\beta E_{\rm surf}}\right)$$

where $E_{\rm surf}$ is the surface electric field in MV/m, β is the surface field enhancement factor, and ϕ is the work function of the metal surface in eV. We note that $\phi = 4$ eV for niobium. For the present study, we assume a well processed cavity with β=100 and scan the cavity surface for field emission at accelerating gradients of 3, 5, and 10 MV/m. The emission from a given site is normalized to a total dissipated power of 1 W for primary electrons, which determines the emitting area A_E in m^2. In other words, $A_E \int J(\theta) E_{\rm kin}(\theta) d\theta = 2\pi$ W, where $J(\theta)$ is the current density determined with the instantaneous field at rf phase θ, $E_{\rm kin}(\theta)$ is the impacting energy of the electron emitted at that phase, and the integration runs from 0 to π or π to 2π depending on the location of the site in the cavity. Average impact energy is determined by $\int J(\theta) E_{\rm kin}(\theta) d\theta / \int J(\theta) d\theta$, and peak energy can be read directly from the output. It turns out that there are two classes of emission sites. One class of emission sites is completely self-contained and can be neglected for the purpose of this study. Also, the nature of π mode is evident in the emerging pattern of trajectories in the remaining sites. Finally, we also note that we have looked at the trajectories of primary and energetically back-scattered secondary electrons only. Our assertion that a given site can not produce electrons landing at a certain location should be understood with such restriction in mind.

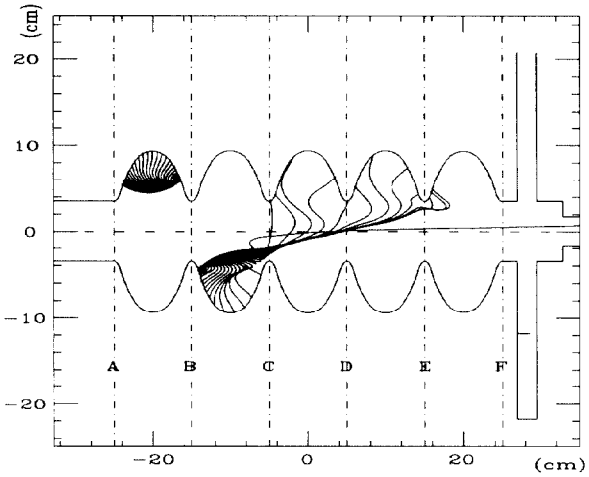

Figure 2. For the gradient range of 3 to 10 MV/m, electrons emitted from the vicinity of A, B, C, D, E, and F only can move to other parts of the cavity, and could in some cases become a dark current. Sample trajectories shown are for 10 MV/m gradient.

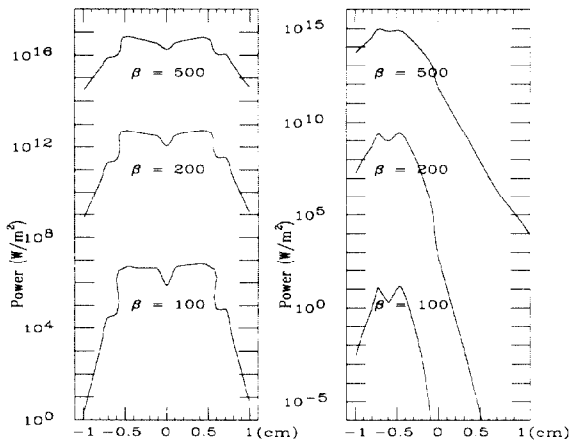

Figure 3. Total dissipated power depends strongly on β; left figure for emission sites near C, and right for sites near F.

A. Electrons Which Can Hit the Cold Window

We find that there are very few emission sites from which electrons can strike the window directly. There are several sites on the short beam pipe section between the end cell and FPC which actually can emit electrons which reach the ceramic window, but the surface field there is below the level we require for an emission site to be of any significance($E_{\rm surf}$ = 3, 5, and 5 MV/m for $E_{\rm acc}$ = 3, 5, and 10 MV/m, respectively). In the case of 10 MV/m gradient, we find five emission sites, which may possibly be direct hit sites, and electrons from there can travel beyond 5 cm from the beam axis into the FPC. We note that

the window is located at 7.9 cm from the beam axis. For lower gradients of 3 and 5 MV/m, only two sites are found in each case. Emission characteristics of those sites are summarized below in Table 1.

Table 1. Possible direct hit sites

Site (cm)	E_{kin} (keV)	J (A/m^2)	$\Delta\theta$ (o)	A_E (m^2)	E_{surf} (MV/m)
10 MV/m					
C−0.5969	672	1.12	0.1	2.18×10^{-5}	19.6
D−0.5969	92	2.13	0.5	1.3×10^{-5}	20.0
D+0.8034	94	1.19×10^{-15}	2.5	1.03×10^{-3}	8.98
D+0.8825	118	5.19×10^{-18}	2.0	1.17×10^{-2}	8.27
E−0.4696	157	0.69	0.25	4.01×10^{-5}	19.3
E+0.7243	92	8.94×10^{-13}	10.0	3.51×10^{-4}	10.0
5 MV/m					
E−0.1174	33	7.60×10^{-14}	0.1	1.74×10^{6}	9.62
F−0.3522	32	2.82×10^{-24}	4.0	4.59×10^{17}	6.63
3 MV/m					
E−0.3522	25	0	0.1	∞	6.09
F−0.4696	16	0	0.5	∞	4.23

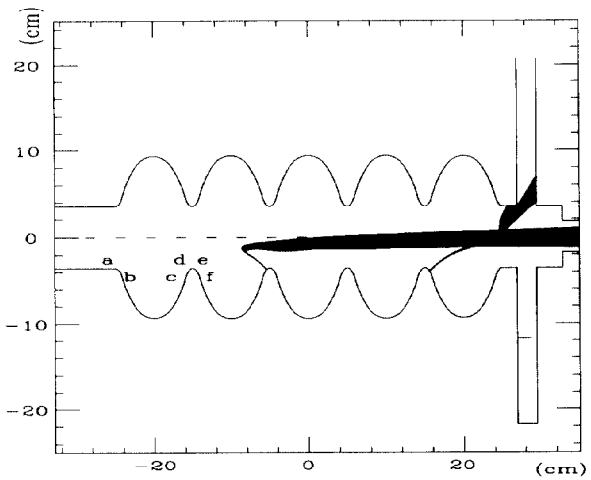

Figure 4. Two field emission sites which contribute to the electron loading of the ceramic window, and to the generation of dark currents, respectively, are shown.

For back-scattered electrons, the impact energy and current of secondary electrons are calculated in a Monte Carlo approach. We notice that each emitting area around noses can further be divided into four subregions(two subregions near A and F). Electrons from two of those subregions(e.g., d and f in Fig. 4) move in general direction toward the FPC side, while field electrons emitted from the remaining two subregions(c and e in Fig. 4) propagate to the opposite end of the cavity. For a given β we also find that the emission from the site d(and from the equivalent site of other cells) is the dominant source of impact power on the window due to the fact that the primary electrons from such a site are produced at the rf phase near 90° at the maximum acceleration. Interesting parameters of back-scattered electrons crossing the window are listed in Table 2 for a few selected emission sites. We note that Table 2 is constructed from trajectories with the cavity gradient of 10 MV/m.

Table 2. Back-scattered electrons

Site (cm)	E_{kin}^{peak} (MeV)	E_{kin}^{avg} (MeV)	I^{peak} (μA)	I^{avg} (μA)	A_E (m^2)
A+0.5969	4.07	2.55	4.78×10^{-6}	3.25×10^{-6}	0.521
B−0.4696	3.78	2.37	6.50×10^{-5}	1.26×10^{-5}	1.71×10^{-6}
C−0.4696	1.97	1.14	4.17×10^{-3}	1.75×10^{-3}	1.93×10^{-7}
D−0.4696	1.47	0.805	2.43×10^{-3}	2.43×10^{-3}	1.55×10^{-7}
E−0.4696	0.759	0.406	0.443	0.243	4.01×10^{-5}
F−0.4696	0.323	0.168	1.06×10^{-2}	1.03×10^{-2}	6.79×10^{-2}

B. Dark Currents

We find that almost every emission site near A, B, C, D, E, and F is a potential source of dark currents with electrons transported out of the cavity when emitted at a proper phase. All possible emission sites have been identified. However, in this report we concentrate on the emission site # 175, to be identified with the site C−0.4696 in Table 2, for the case of 10 MV/m gradient(a factor of 2 above design gradient). This site turned out to be one of the strongest sources of field emission for the CEBAF cavity. Electron trajectories from this site moving parallel to the beam axis are shown in Fig. 4. We find that electrons emitted at phases between 105 and 111° can form a bunch with bunch length = 12.6 ps, energy = 3.32 MeV, energy spread (rms) = 52.7 keV, bunch charge = 0.03 fC, and angular spread (half width) = 14.5 mrad. Half beam width of 1 cm at the narrow beam pipe is required for trajectories which form the bunch. Transverse phase space at this point has a slope of 1.5 mrad/mm and an angular offset of 14.5 mrad. Average current is estimated to be 45.6 nA when $A_E = 1.93\times10^{-7}$ m^2 is used. This indeed can cause a significant background problem to Hall B experiments, if transmitted. However, it is expected that forward moving field emitted currents from the linacs will be intercepted at the spreaders(and backward currents at the recombiners, respectively) because of low energy acceptance of less than one percent level of such beam transport modules. On the other hand, dark currents from injector cryomodules need to be stopped at the injector chicane. The effectiveness of transport elements in blocking dark current transmission merits further study.

V. REFERENCES

[1] I. Ben-Zvi, J. F. Crawford, and J. P. Turneaure, *IEEE Trans. Nucl. Sci.* **NS-18**, 166 (1971).

[2] R. Klatt *et al.*, *Proc. 1986 Linear Accelerator Conf.*, 276 (1986).

[3] B. C. Yunn, "URMEL/URMELT Study of the CEBAF/CORNELL Cavity," unpublished.

[4] J. C. Amato, "Summary of HOM measurements to date," Cornell Univ. LNS report, SRF-831002 (1983).

[5] R. H. Fowler and L. Nordheim, *Proc. R. Soc. London* **A119**, 173 (1928).